Stanford Exploration Project, Report 115, May 22, 2004, pages 1–12

Imaging overturned waves by plane-wave migration in tilted coordinates

Guojian Shan and Biondo Biondi[1]

ABSTRACT

We image overturned waves by decomposing the source and receiver wavefields into plane-waves. For each plane-wave, we extrapolate the source and receiver wavefields in a tilted coordinate system and cross-correlate them to obtain Common Image Gathers (CIGs). The tilting angle for the coordinate system is determined by the propagation direction of the plane wave. In tilted coordinates, the propagation direction is close to the extrapolation direction, so we can image steeply dipping reflectors and overturned waves with the one-way wave equation. We can also obtain robust, dip-dependent angle-domain CIGs (ADCIGs) by the same method employed in reverse-time migration. These gathers provide moveout information and thus are very important for velocity analysis on steeply dipping reflectors. Since plane-wave migration needs no padding and the extrapolation is one-way wave equation based, our method is very efficient. We demonstrate our method on the Marmousi model by computing the Green's function for a point source on the surface. We also apply our method to a North Sea real dataset with overturned events.

INTRODUCTION

Downward continuation migration (Claerbout, 1985) increases in popularity with the continuing development of computer power. It is accurate, and can handle lateral velocity change and multi-pathing naturally. It is used to image complex geological structure, especially sub-salt reflectors. However, the dip angle of reflectors is limited in downward continuation, which makes it difficult to image steeply dipping reflectors and overturned waves. Downward continuation is based on the one-way wave equation and extrapolates the wavefields in the downward direction, although in reality, waves propagate in all directions. When the propagation direction of waves is too far from the extrapolation direction, the accuracy of extrapolation is limited.

Kirchhoff methods can handle steeply dipping reflectors and overturned waves, but they are based on a high-frequency approximation and are less reliable for imaging complex geological structure, where multi-path events are present. Reverse-time migration (Whitmore, 1983; Baysal et al., 1983; Biondi and Shan, 2002), which is based on the two-way wave equation, can handle waves propagating in all directions, but it is still too expensive for today's

[1]**email:** shan@sep.stanford.edu, biondo@sep.stanford.edu

computer power.

Many methods have been developed to handle waves that propagate at large angles to the extrapolation direction. They solve the problem either by developing a more accurate extrapolation operator to image high-angle waves, such as Fourier finite difference (Ristow and Ruhl, 1994; Biondi, 2002) and generalized screen propagators (de Hoop, 1996; Huang and Wu, 1996), or by making the extrapolation direction closer to the propagation direction, such as beam migration (Hill, 2001; Gray et al., 2002; Albertin et al., 2001; Brandsberg-Dahl and Etgen, 2003), beamlet migration (Chen et al., 2002) and coordinate-transformation based methods (Zhang and McMechan, 1997; Etgen, 2002; Sava and Fomel, 2004). Our method is of the latter type. We decompose both source and receiver wavefields into plane-waves and run plane-wave migration (Rietveld, 1995; Duquet et al., 2001; Liu et al., 2002; Zhang et al., 2003) on each of them within a tilted coordinate system (Etgen, 2002).

Offset-domain CIGs for shot-profile migration and reverse-time migration are generated by cross-correlating the source and receiver wavefields with a horizontal shift (Rickett and Sava, 2002), and can be transformed into ADCIGs by slant stack (Sava and Fomel, 2003). However, CIGs obtained from downward continuation are contaminated by smearing noise at steeply dipping reflectors (Biondi and Shan, 2002). Reverse-time migration can provide both horizontal and vertical CIGs. Both are then merged into dip-dependent CIGs, which are robust and immune to the smearing noise (Biondi and Symes, 2003). By performing plane-wave migration in tilted coordinates, we can obtain similar dip-dependent ADCIGs. These CIGs are robust and are useful for velocity analysis in the presence of steeply dipping reflectors in the subsurface.

TILTED CARTESIAN COORDINATES

In Cartesian coordinates (x,z), the one-way wave equation is

$$\frac{\partial P}{\partial z} = \frac{i\omega}{v}\sqrt{1+\frac{v^2}{w^2}\frac{\partial^2}{\partial x^2}}P. \tag{1}$$

It can be obtained by factoring the two-way acoustic wave equation. If the coordinates are rotated by an angle θ, the two-way acoustic wave equation doesn't change in the new coordinates (x',z'). Factoring the two-way wave equation in the tilted coordinates, we can obtain the same one-way wave equation. In the tilted coordinates, wavefields are now extrapolated in the z' direction, rather than in the downward direction as done in downward continuation. Also the source and receiver data are not on the line $z'=0$, but on $x'\sin\theta - z'\cos\theta = 0$ (Figure 1a).

For a point source, the waves propagate in all directions, making it impossible to cover all propagation directions with only one Cartesian coordinate system. We decompose the point source into plane waves and extrapolate each plane wave in tilted coordinates, whose extrapolation direction z' is determined by the propagation direction of the plane wave. The propagation direction of the plane wave at the surface can be used as the extrapolation direction

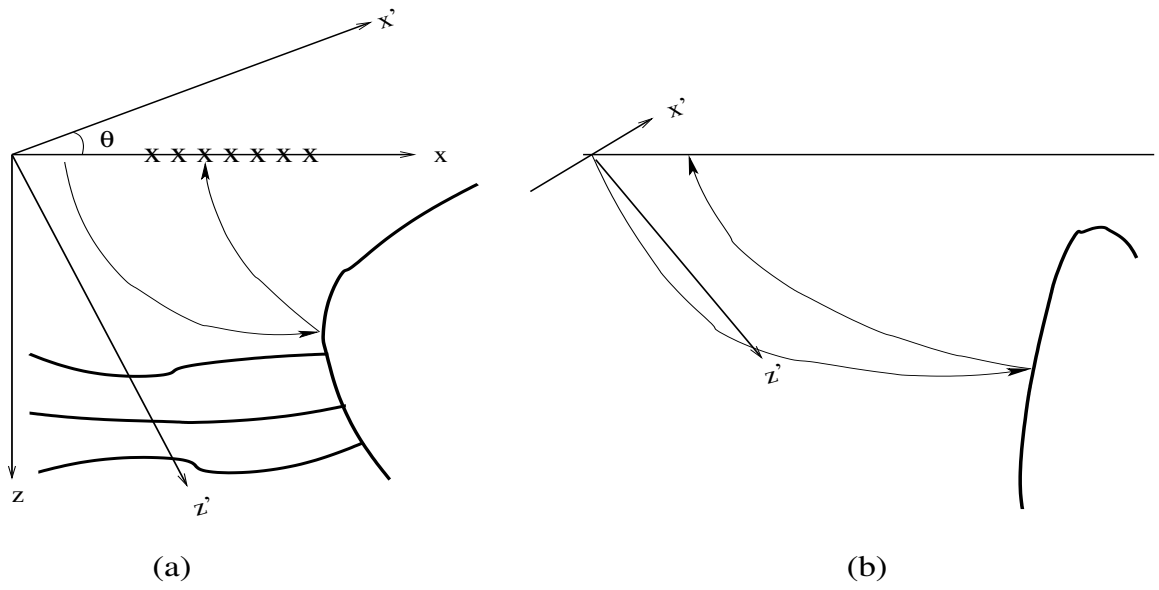

Figure 1: Tilted Cartesian coordinates: (a) sources and receivers are on the line $x'\sin\theta - z'\cos\theta = 0$ and the extrapolation direction is the z' direction; (b) sources and receivers are usually very far from the reflection point for overturned waves and the opening angle is usually small. guojian1-tilt [NR]

z' of the tilted coordinates. In this coordinate system, the source and receiver wavefields of overturned waves can usually be caught, since the opening angle between them is usually small and the propagation directions of the source and receiver wavefields are close to each other (Figure 1b).

Another advantage of using a plane-wave rather than a point source is that no padding is needed to image steeply dipping reflectors. To catch the energy from steeply dipping reflectors, the locations of sources and receivers are usually far from the reflector point (Figure 1b). Large extrapolation aperture is required to image these reflectors using a point-source method. In contrast, plane waves inherently have large apertures, which can easily cover the locations of source, receiver and reflector points. This greatly reduces the cost of imaging the steeply dipping reflectors.

ANGLE-DOMAIN CIGS IN TILTED CARTESIAN COORDINATES

In shot-profile migration, offset-domain CIGs can be obtained by cross-correlating the source and receiver wavefields with a horizontal shift (Rickett and Sava, 2002). The offset-domain CIGs can be transformed into ADCIGs by slant-stack (Sava and Fomel, 2003). In reverse-time migration, in addition to horizontal offset-domain CIGs, we have vertical offset-domain CIGs, which are obtained by cross-correlating the source and receiver wavefields with a vertical shift (Biondi and Shan, 2002). Both horizontal and vertical offset-domain CIGs can be transformed into ADCIGs and merged into dip-dependent CIGs, by transforming the horizontal and vertical

offsets into apparent geological offset as follows (Biondi and Symes, 2003):

$$h_x = \frac{h_0}{\cos\alpha}, \tag{2}$$

$$h_z = \frac{h_0}{\sin\alpha}, \tag{3}$$

where α is the dip angle of the subsurface reflector, h_x is the horizontal offset, h_z is the vertical offset and h_0 is the apparent geological offset.

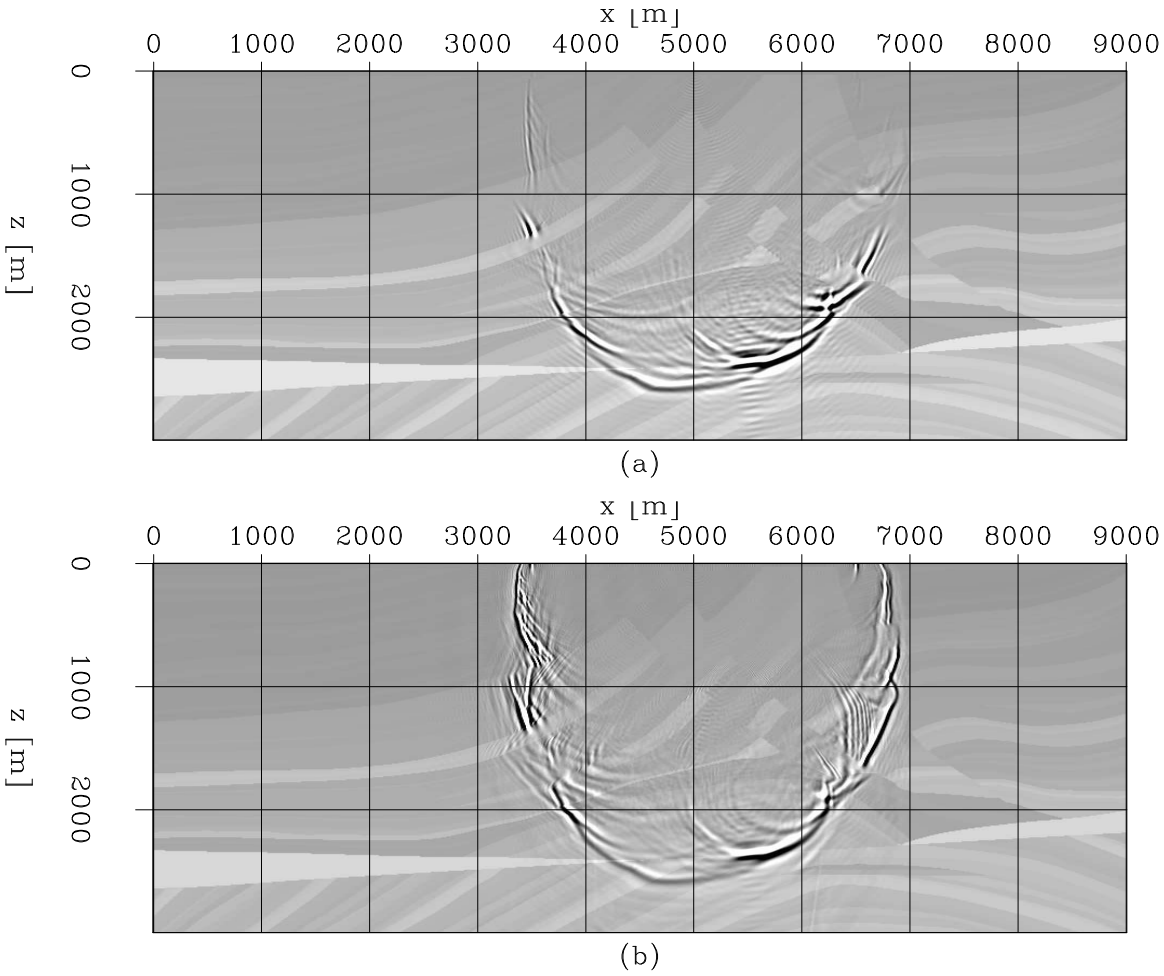

Figure 2: The Marmousi model: (a) wavefields obtained by downward continuation with FFD; (b) wavefields obtained by plane-wave decomposition and extrapolation in tilted coordinates. guojian1-mar.green [CR]

In the tilted coordinates, wavefields are extrapolated in the z' direction. The offset-domain CIGs are generated by cross-correlating the source and receiver wavefields with an x' direction shift. So the subsurface offset is in the x' direction. As with the apparent geological offset h_0,

the x' direction offset $h_{x'}$ can be transformed to horizontal and vertical offsets as follows:

$$h_x = \frac{h_{x'}}{\cos\theta}, \tag{4}$$

$$h_z = \frac{h_{x'}}{\sin\theta}, \tag{5}$$

where θ is the tilting angle in Figure 1. As for reverse-time migration, horizontal and vertical offset-domain CIGs can be transformed into ADCIGs and merged into dip-dependent ADCIGs. A simple way to merge them is with the following weights:

$$w_{h_x} = \cos^2\alpha, \tag{6}$$

$$w_{h_z} = \sin^2\alpha, \tag{7}$$

where α is the apparent dip angle of the reflector. Dip-dependent residual moveout (Shan and Biondi, 2003) can be used to analyze dip-dependent ADCIGs to provide useful moveout information for velocity analysis.

In tilted coordinates, the direction of subsurface offset is close to that of apparent geological offset, since the extrapolation direction of the wavefields is close to the propagation direction of the waves. Within a limited length of subsurface offsets, we can obtain much more accurate CIGs at steeply dipping reflectors than with standard downward continuation.

EXAMPLES

Our first example concerns waves propagating in the Marmousi model. Figure 2 presents (a) the wavefields obtained by downward continuation with Fourier finite difference (FFD) overlaid velocity model, and (b) the wavefields obtained by plane-wave decomposition and extrapolation of each plane wave with FFD in tilted coordinates overlaid velocity model. The source location is at $x = 5000$m, and the traveltime is 3s. In Figure 2a, although we extrapolate the wavefield with a wide-angle extrapolation operator, the wavefield is not accurate for large incident angles. In contrast, Figure 2b does not have this angle limitation, and the wavefield is extrapolated better for high-angle waves.

Our second example images the overturned waves of a 2-D line from the ELF L7D North Sea dataset. This dataset presents challenges caused by the interaction between the salt edge and a chalk layer. The migration velocity is a smooth version of a tomographic result, which was obtained by inverting the moveouts measured on ADCIGs computed from downward-continuation prestack migration (Clapp, 2001). The image from reverse-time migration (Biondi and Shan, 2002) shows the presence of overturned energy. Figure 3 shows (a) the image obtained by downward continuation, (b) the image obtained by reverse-time migration, (c) the image obtained by plane-wave migration in tilted coordinates and (d) the rays shot from the steeply dipping reflector. Note that, to save computational cost, we use large space-sampling in reverser-time migration, which make reflectors in Figure 3b not as continuous as the others. There are two steeply dipping reflectors at the edge of the salt, one of which is almost vertical. Rays from these two reflectors (Figure 3d) show that the waves are overturned.

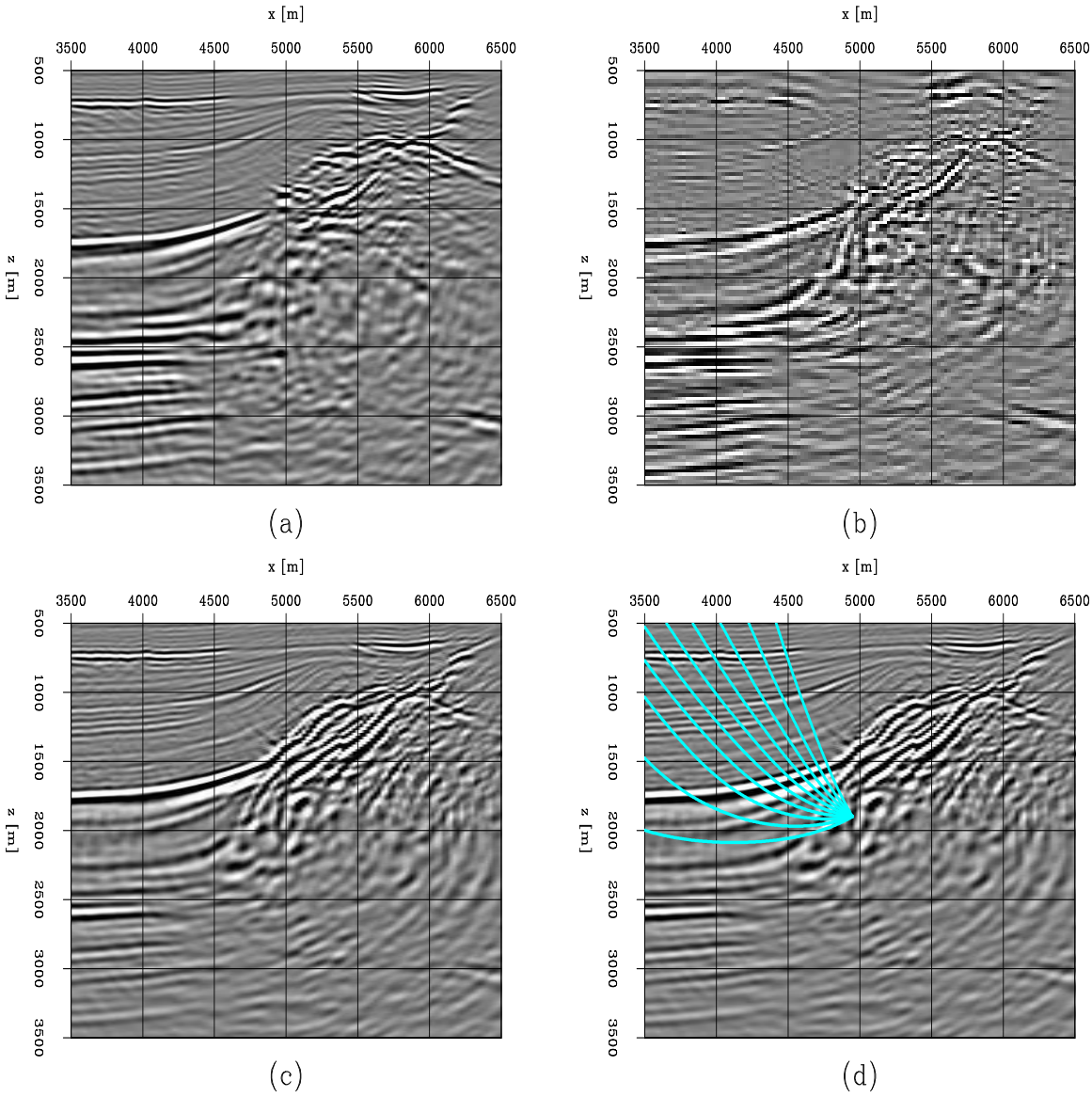

Figure 3: Migration of North Sea real dataset: (a) the image from downward continuation; (b) the image from reverse-time migration; (c) the image from plane-wave migration in tilted coordinates; (d) the rays shot at $x = 5000$m, $z = 1900$m. guojian1-elf.image [CR]

Downward continuation (Figure 3a) doesn't image these two steeply dipping reflectors, failing to handle the overturned energy. In contrast, both reverse-time prestack migration (Figure 3b) and plane-wave migration in tilted coordinates (Figure 3c) preserve the overturned energy and image the steeply dipping reflectors. The images of the steep reflectors by these two methods are comparable, but the cost of plane-wave migration in tilted coordinates is much less than that of reverse-time migration.

Figure 4 compares the horizontal CIGs at the surface location $x = 4000$m from plane-wave migration in tilted coordinates with those from reverse-time migration. Figure 4a and Figure 4c show offset and angle domain CIGs from reverse-time migration, respectively. Figure 4b and Figure 4d show offset and angle domain CIGs from plane-wave migration in tilted coordinates, respectively. The ADCIGs from plane-wave migration in tilted coordinates look similar to those from reverse-time migration.

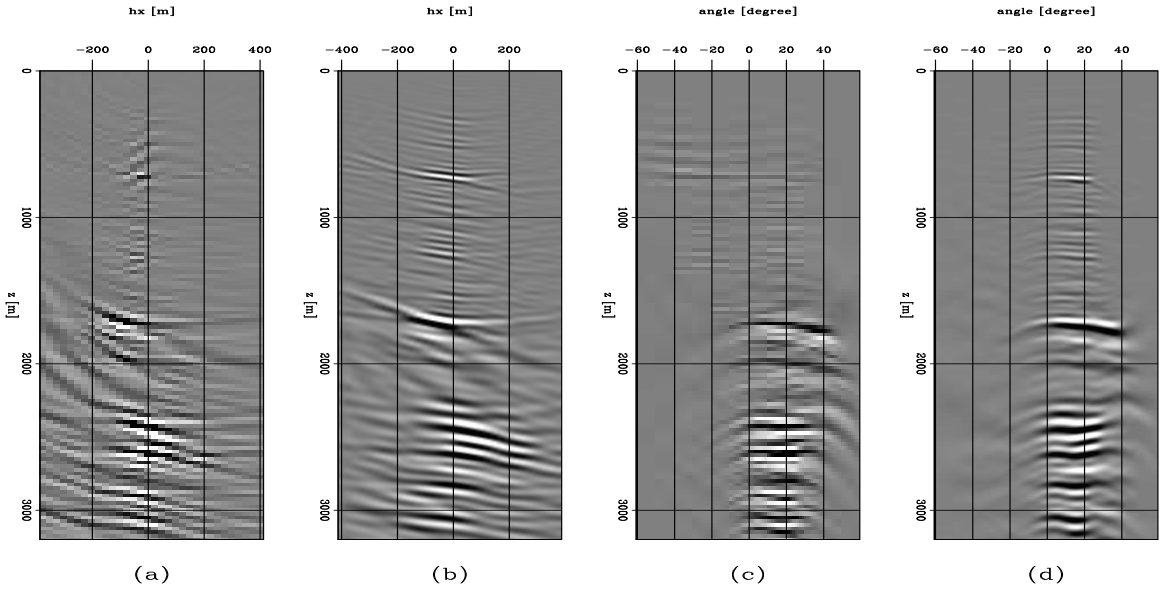

Figure 4: Horizontal CIGs at $x = 4000$m: (a) offset-domain CIGs obtained by reverse-time migration; (b) offset-domain CIGs obtained by plane-wave migration in tilted coordinates; (c) ADCIGs obtained by reverse-time migration; (d) ADCIGs obtained by plane-wave migration in tilted coordinates. guojian1-elf.cig [CR]

Figure 5 compares the horizontal CIGs at the surface location $x = 5000$m from plane-wave migration in tilted coordinates with those from reverse-time migration. Panels are organized as in Figure 4. The vertical salt edge is located at surface location x=5000m, in the vertical interval $1500 < z < 2000$m. At the vertical salt edge, we show that the ADCIGs from reverse-time migration and from plane-wave migration in tilted coordinates are similarly smeared along the angle axis. This smearing noise makes horizontal CIGs a poor source of information for velocity analysis at these steeply dipping reflectors.

Figure 6 compares the vertical CIGs at depth $z = 1900$m from plane-wave migration in tilted coordinates with those from reverse-time migration. Panels are organized as in Figure

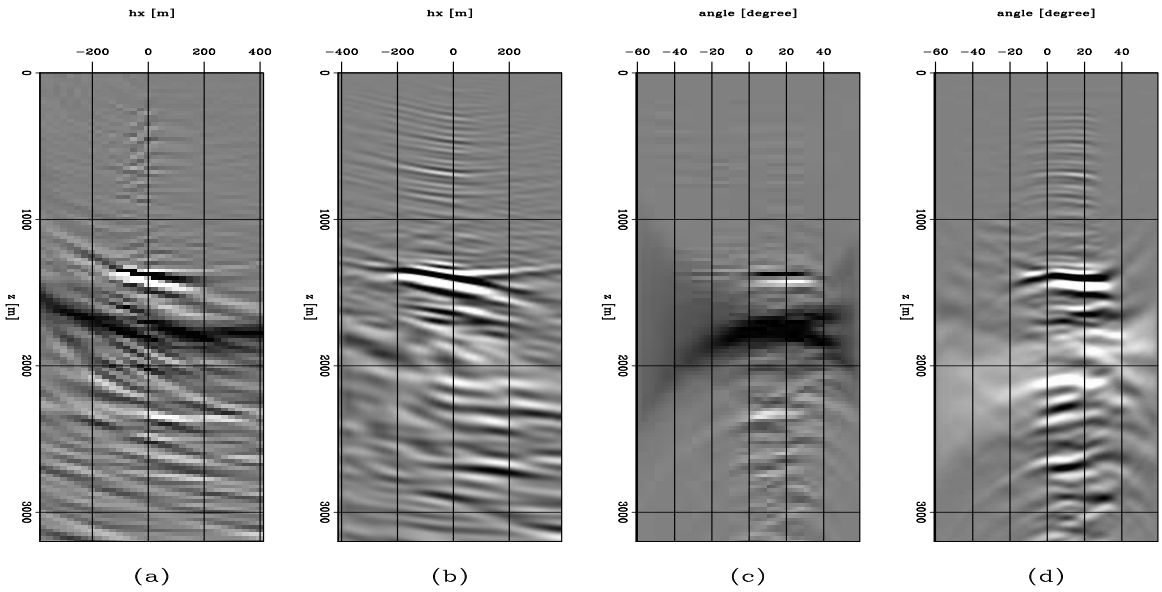

Figure 5: Horizontal CIGs at $x = 5000$m: (a) offset-domain CIGs obtained by reverse-time migration; (b) offset-domain CIGs obtained by plane-wave migration in tilted coordinates; (c) ADCIGs obtained by reverse-time migration; (d) ADCIGs obtained by plane-wave migration in tilted coordinates. guojian1-elf.cig.5000 [CR]

4 but in the vertical direction. The vertical ADCIGs from both methods are similar. In contrast to horizontal CIGs, vertical CIGs focus at the vertical salt edge and can provide useful information for velocity analysis at the salt edge.

Figure 7 shows the dip-dependent ADCIGs obtained by merging horizontal and vertical ADCIGs with the weights in equations (6) and (7). Comparing against horizontal and vertical ADCIGs, we find that dip-dependent ADCIGs are more robust. The smearing noise is avoided and both horizontal and vertical reflectors are well focused.

CONCLUSION

We image the overturned waves by decomposing the source and receiver wavefields into plane waves. Each plane wave is extrapolated in tilted Cartesian coordinates. Offset-domain CIGs are generated by cross-correlating the source and receiver wavefields, with a shift in the direction normal to the extrapolation direction. The offset-domain CIGs are decomposed into horizontal and vertical CIGs, which are merged into robust, dip-dependent ADCIGs.

We apply our method to a North Sea dataset and compare the image with the ones obtained from downward continuation and reverse-time migration. The image obtained by plane-wave migration in tilted coordinates is better than the image obtained from standard downward continuation. The steeply dipping salt edge is imaged by one-way plane-wave migration in tilted coordinates, but it is missing in the image obtained by downward continuation. The

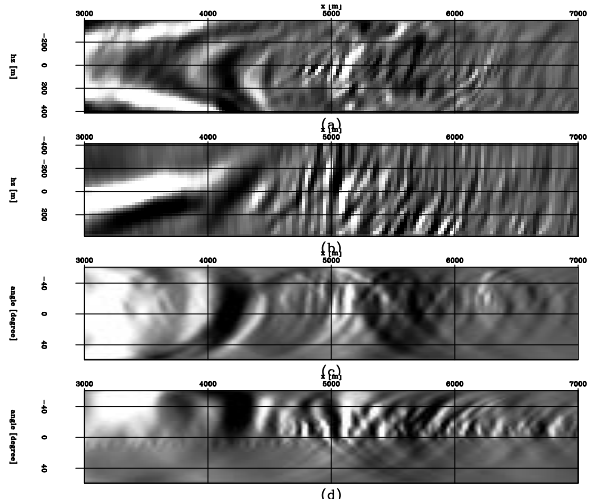

Figure 6: Vertical CIGs at $z = 1850$m: (a) offset domain CIGs obtained by reverse-time migration; (b) offset domain CIGs obtained by plane-wave migration in tilted coordinates; (c) ADCIGs obtained by reverse-time migration; (d) ADCIGs obtained by plane-wave migration in tilted coordinates. guojian1-elf.hz.cig [CR]

plane-wave migration results are also comparable to those obtained by reverse-time migration and produces similar horizontal and vertical CIGs, while its computational cost is much less than reverse-time migration. The dip-dependent ADCIGs merged from horizontal and vertical CIGs are robust and provide useful moveout information for reflectors with a wide range of dips.

ACKNOWLEDGMENTS

We would like to thank TotalFinalElf for making the North Sea dataset available.

REFERENCES

Albertin, U., Yingst, D., and Jaramillo, H., 2001, Comparing common-offset Maslov, Gaussian beam, and coherent state migrations: Soc. of Expl. Geophys., 71st Ann. Internat. Mtg, 913–916.

Baysal, E., Kosloff, D. D., and Sherwood, J. W. C., 1983, Reverse time migration: Geophysics, **48**, no. 11, 1514–1524.

Biondi, B., and Shan, G., 2002, Prestack imaging of overturned reflections by reverse time migration: Soc. of Expl. Geophys., 72nd Ann. Internat. Mtg, 1284–1287.

Biondi, B., and Symes, W., 2003, Wavefield-continuation angle-domain common-image gathers for migration velocity analysis: Soc. of Expl. Geophys., 73rd Ann. Internat. Mtg., 2104–2107.

Biondi, B., 2002, Stable wide-angle Fourier finite-difference downward extrapolation of 3-D wavefields: Geophysics, **67**, no. 03, 872–882.

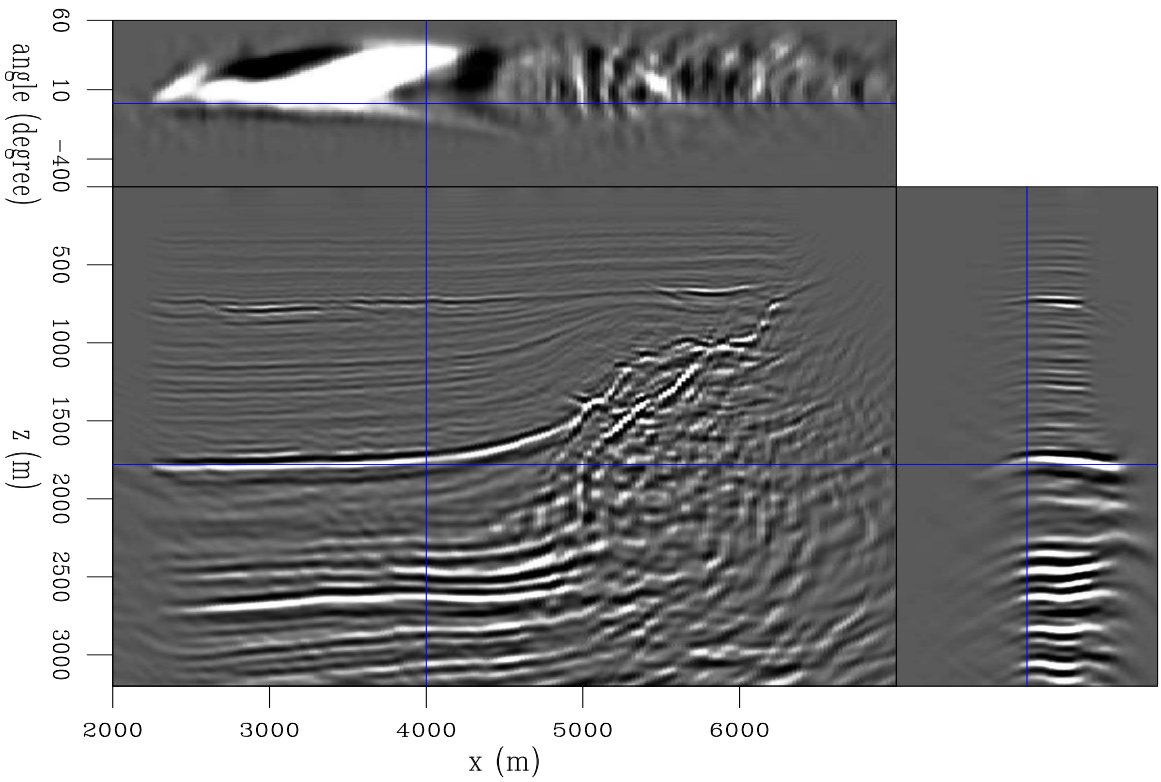

Figure 7: Dip-dependent ADCIGs: Notice that both horizontal and vertical reflectors are focused very well. guojian1-ang.image.elf.dip [CR]

Brandsberg-Dahl, S., and Etgen, J., 2003, Beam-wave imaging: Soc. of Expl. Geophys., Expanded Abstracts, 977–980.

Chen, L., Chen, Y., and Wu, R., 2002, Target-oriented prestack beamlet migration using Gabor-Daubechies frames: Soc. of Expl. Geophys., 72nd Ann. Internat. Mtg, 1356–1359.

Claerbout, J. F., 1985, Imaging the Earth's Interior: Blackwell Scientific Publications.

Clapp, R. G., 2001, Geologically constrained migration velocity analysis: Ph.D. thesis, Stanford University.

de Hoop, M. V., 1996, Generalization of the Bremmer coupling series: Generalization of the Bremmer coupling series:, J. Math. Phys., 3246–3282.

Duquet, B., Lailly, P., and Ehinger, A., 2001, 3-D plane wave migration of streamer data: Soc. of Expl. Geophys., 71st Ann. Internat. Mtg, 1033–1036.

Etgen, J., 2002, Waves, beams and dimensions: an illuminating if incoherent view of the future of migration: 72nd Ann. Internat. Mtg, Soc. of Expl. Geophys., invited presentation.

Gray, S., Notfors, C., and Bleistein, N., 2002, Imaging using multi-arrivals: Gaussian beams or multi-arrival Kirchhoff?: Soc. of Expl. Geophys., 72nd Ann. Internat. Mtg, 1117–1120.

Hill, N. R., 2001, Prestack Gaussian-beam depth migration: Geophysics, **66**, no. 4, 1240–1250.

Huang, L. Y., and Wu, R. S., 1996, Prestack depth migration with acoustic screen propagators: Soc. of Expl. Geophys., 66th Ann. Internat. Mtg, 415–418.

Liu, F., Stolt, R., Hanson, D., and Day, R., 2002, Plane wave source composition: An accurate phase encoding scheme for prestack migration: Soc. of Expl. Geophys., 72nd Ann. Internat. Mtg, 1156–1159.

Rickett, J. E., and Sava, P. C., 2002, Offset and angle-domain common image-point gathers for shot-profile migration: Geophysics, **67**, no. 03, 883–889.

Rietveld, W. E. A., 1995, Controlled illumination of prestack seismic migration: Delft University of Technology., Ph.D. thesis.

Ristow, D., and Ruhl, T., 1994, Fourier finite-difference migration: Geophysics, **59**, no. 12, 1882–1893.

Sava, P. C., and Fomel, S., 2003, Angle-domain common-image gathers by wavefield continuation methods: Geophysics, **68**, no. 3, 1065–1074.

Sava, P., and Fomel, S., 2004, Wavefield extrapolation in Riemannian coordinates: Soc. of Expl. Geophys., Expanded Abstracts.

Shan, G., and Biondi, B., 2003, Dip-dependent residual moveout: SEP–**114**, 95–100.

Whitmore, N. D., 1983, Iterative depth migration by backward time propagation: Soc. of Expl. Geophys., 53rd Ann. Internat. Mtg, Session:S10.1.

Zhang, J., and McMechan, G. A., 1997, Turning wave migration by horizontal extrapolation: Geophysics, **62**, no. 01, 291–297.

Zhang, Y., Sun, J., Notfors, C., and Gray, S., 2003, Delayed-shot 3-D prestack depth migration: Soc. of Expl. Geophys., Expanded Abstracts, 1027–1030.